Nano Energy 126 (2024) 109656

Contents lists available at ScienceDirect

Nano Energy

journal homepage: www.elsevier.com/locate/nanoen

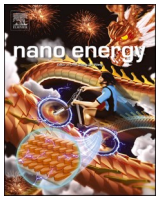

Modulating local environment for electrocatalytic CO_2 reduction to alcohol

Chaojie Chen, Linsen Huang, Yunling Jiang, Yao Zheng *, Shi-Zhang Qiao *

School of Chemical Engineering, The University of Adelaide, Adelaide, SA 5005, Australia

ARTICLE INFO

Keywords:
CO_2 reduction reaction
Local reaction environment
C_2H_5OH production
Interfacial *CO/*H coverage

ABSTRACT

The fundamental drivers for the selective CO_2 electroreduction reaction (CO_2RR) to alcohol (e.g. C_2H_5OH) or alkene (e.g. C_2H_4) still remain unexplored. Previous studies mainly focus on catalyst engineering to enhance electrocatalytic performance, while the selectivity to alcohol has reached a bottleneck. Here, we modulate local environment to reveal the contribution of *CO and *H reaction intermediates in the selectivity of CO_2 to alcohol/alkene on Cu electrocatalyst. Through modifications on local CO_2 concentration, varied *CO/*H coverage ratios can be achieved. Based on the reaction kinetics analysis, we find that there is a direct connection between local CO_2 concentration and interfacial *CO and *H coverage, which finally affects the selectivity of CO_2 to alcohol or alkene. To verify this principle, polyvinylidene fluoride (PVDF), a hydrophobic binder, were selected and introduced into the catalyst surface for further enhancement of interfacial *CO/*H coverage. With PVDF decoration, alcohol/alkene ratio increased from 0.69 to 1.35. The Faradic Efficiency of alcohol is up to 37.5 % under a high current density of 800 mA cm^{-2} (a partial current density of 300 mA cm^{-2}), surpassing most reported Cu-based materials. Our findings provide a fundamental guidance for CO_2RR to alcohol under an industrial-level current density.

1. Introduction

The electrochemical carbon dioxide reduction reaction (CO_2RR) has emerged as a pivotal avenue for converting CO_2 into value-added products, holding significant promise in addressing climate change concerns [1–3]. However, a high selectivity to single C_{2+} products is still a grand challenge, which is a key factor in reaching the goal of industrial CO_2 electrolysis [4–6]. Among diverse valuable C_{2+} products, alkene (ethylene, C_2H_4) and alcohol (ethanol, C_2H_5OH and propanol, C_3H_7OH) stand out as predominant categories. Due to a relatively lower energy barrier for the C_2H_4 formation process, it is possible to achieve an exceptional selectivity of C_2H_4 (e.g. 70 % at –0.55 V vs. RHE) [7–9]. Nevertheless, a high selectivity to liquid alcohols still presents as a challenge. Furthermore, fundamental drivers for the alcohol production remain inadequately investigated and it is also the issue that limits commercialization of CO_2RR.

Nowadays, various catalysts engineering strategies, including nanostructure [10], tandem structure [11], and single atom [12], are employed to enhance the alcohol production on Cu-based electrocatalysts. In these systems, catalysts' intrinsic properties, such as wettability of protective layers [13] and nanosized catalyst structure [14], are proposed as drivers for ethanol formation. However, these approaches mainly depend on the electronic structures of designed materials, demonstrating that proposed drivers are unsuitable for extrapolation to other materials [15–17]. The catalyst's structure significantly determines electrocatalytic performance and even slight change in the structure will result in the complex alterations at the interface. These changes ultimately hinder the explorations of basic descriptors. Conversely, modulating local reaction environment, as a neglected but essential method, can tune interfacial condition individually. The fundamental research based on modifications of local environment can reveal descriptors that are independence of catalyst' structures [18,19]. Therefore, such descriptors can be universal for the enhancement of selectivity.

Herein, through systemically modulating local reactants concentrations, we evaluate interfacial *CO/*H coverage acting as fundamental drivers in the electrochemical CO_2RR to valuable alcohol products. Under varied interfacial CO_2 partial pressures, differential interfacial coverage of *CO/*H intermediates can be observed. The electrocatalytic results demonstrate that the increased *CO can accelerate the alcohol formation, while the enhanced *H is beneficial for the selectivity to alkene. By combining *operando* characterizations with kinetics analysis, we establish a connection between the *CO/*H coverage and the selectivity to alcohol. Under the guidance of this principle, we

* Corresponding authors.
E-mail addresses: yao.zheng01@adelaide.edu.au (Y. Zheng), s.qiao@adelaide.edu.au (S.-Z. Qiao).

https://doi.org/10.1016/j.nanoen.2024.109656
Received 27 February 2024; Received in revised form 10 April 2024; Accepted 21 April 2024
Available online 22 April 2024

incorporate a hydrophobic binder (polyvinylidene difluoride, PVDF) into the catalyst inks. The addition serves to reduce interfacial *H coverage, resulting in an enhanced *CO/*H ratio and a notable selectivity of 37.5 % to alcohol at 800 mA cm^{-2} operation.

2. Result and discussion

2.1. Characterizations of *CO/*H coverage at different P_{CO2}

Modulating local reaction environment can adjust single interfacial factor without affecting catalyst structure, which can be an effective method in mechanism analysis. In this experiment, we systematically tuned the volume ratios of CO_2 to Ar in the gas streams to maintain diverse local reactant concentrations. According to Henry's law, interfacial CO_2 concentration is in positive relation with partial pressure [20]. Therefore, varied interfacial CO_2 partial pressure (P_{CO_2}, ranging from 0.25 to 1) can be achieved.

To assess the alterations in *CO coverage, *in-situ* Attenuated Total Reflectance Infrared (ATR-IR) spectra analysis was conducted in a three-electrode cell at specific potentials. A peak locating around 1948 cm^{-1}, which corresponds to *CO, is detected at –0.9 V vs. RHE under each P_{CO_2} (Fig. 1**a**) [21]. As for spectra collected under P_{CO_2} ranging from 0.25 to 0.75, the *CO peak does not become apparent until under a high negative potential (–0.5 V vs. RHE). In contrast, a well-defined peak can be clearly observed at a moderate potential (–0.1 V vs. RHE) under P_{CO_2}=1. It should be mentioned that the potential for the appearance of *CO peak is smaller with the increase of interfacial P_{CO_2} [22]. Taking spectra gathered at –0.9 V vs. RHE as an example, it is evident that *CO peak intensity substantially increases with a rising P_{CO_2}, confirming a heightened *CO coverage (Fig. S1) [23]. The *H is derived from water splitting, and is in direct competition with *CO adsorption [24,25]. According to *in-situ* Electron Paramagnetic Resonance (EPR) spectra, nine characteristic peaks can be clearly observed under each P_{CO_2} (Fig. 1**b**) [26,27]. With the increase of CO_2 content in the gas streams, the peak intensity obviously decreases, indicating a reduction in the *H coverage. For a quantitative analysis, we introduced a parameter R_c, which is calculated as the ratio of normalized ATR-IR intensity to normalized EPR intensity, to quantify interfacial *CO/*H ratios. As displayed in Fig. 1**c**, an increase of R_c from 0.02 to 3.34 can be observed with the increase of P_{CO_2}, demonstrating an enhanced *CO coverage and decreased *H coverage (Fig. S2). It can be concluded that modulating interfacial CO_2 concentration can achieve a varied interfacial *CO/*H coverage without influence on the catalyst's electronic structure.

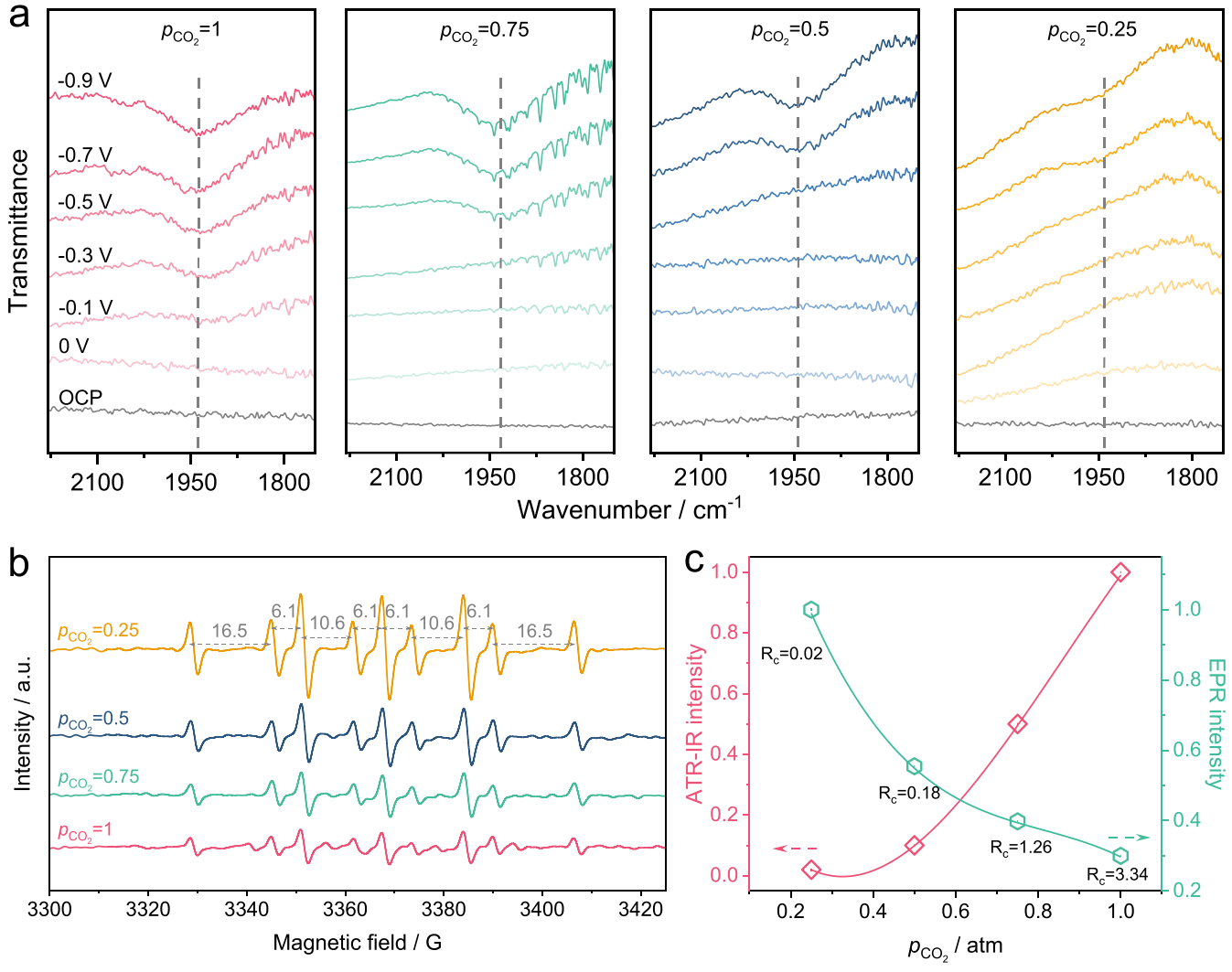

Fig. 1. Characterizations of *CO/*H coverage. (a) The *in-situ* Attenuated Total Reflectance Infrared (ATR-IR) spectra of commercial Cu at specific potentials under varied P_{CO_2} in the 1 M $KHCO_3$ without CO_2-saturated. (b) *Operando* Electron Paramagnetic Resonance (EPR) spectra collected in 1 M $KHCO_3$ solution with 8 μL 5,5-dimethyl-1-pyrroline N-oxide (DMPO) under 200 mA cm^{-2} (30 min reduction). (c) Correlation between P_{CO_2} and normalized ATR-IR intensity and normalized EPR intensity.

2.2. Alcohol/alkene selectivity dependence on *CO/*H coverage

To quantify the dependence of alcohol/alkene selectivity on the *CO/*H coverage, the CO_2RR performances of commercial Cu were evaluated in a flow cell device with 1 M KOH aqueous electrolyte (Fig. S3 and S4). An obvious change on partial H_2 current densities (j_{H_2}) were observed through the regulation of P_{CO_2} (Fig. S5 and S6). Under a current density of 500 mA cm^{-2}, j_{H_2} reaches a maximum value of 266 mA cm^{-2} at P_{CO_2}=0.25, while it delivers a minimum value with increasing P_{CO_2} to 1. As the selectivity to H_2 is positively related with *H coverage, this trend demonstrates a correlation between an increase in interfacial *H coverage and a decrease in P_{CO_2}, which is consistent with our *operando* characterization results. [28]

Fig. 2**a** compares the Faradic Efficiency (FE) of C_{2+} alcohol (C_2H_5OH and C_3H_7OH) and alkene (C_2H_4) products. With the increase in P_{CO_2}, FEs of C_{2+} alcohol and alkene enhance from 16 % to 60 % (500 mA cm^{-2}). Interestingly, at a low reaction rate (100 mA cm^{-2}), the catalyst delivers a high alkene selectivity of 40 % at P_{CO_2}=0.25. At high reaction rates (200, 300 mA cm^{-2}), FE_{alk} reaches a maximum value with the existence of trace amount of *H. Meanwhile, with increasing current density, the peak position for j_{alk} (alkene partial current densities) gradually shifts to a higher P_{CO_2} (Fig. 2**b**, Fig. S7). It should be noticed, for alcohol products, partial current densities of alcohol products (j_{alc}) increase with the enhancement in P_{CO_2}, suggesting a promotive influence of interfacial *CO on alcohol selectivity (Fig. 2**c**, Fig. S8). Meanwhile, according to chronopotentiometry (CP) curves at 200 mA cm^{-2}, evident potential fluctuations can be observed for curves collected at P_{CO_2}=0.25 and 0.5 (Fig. S9). As exhibited in Fig. S10, a rising P_{CO_2}, which corresponds to higher *CO coverage and lower *H coverage, accelerates the formation of alcohol, and inhibits the selectivity to alkene products. The influence of *CO/*H on alcohol/alkene selectivity is further supported by plotting the ratio of FE_{alc} to FE_{alk} (FE_{alc}/FE_{alk}) as a function of P_{CO_2} at various current densities (Fig. 2**d**). The FE_{alc}/FE_{alk} increases from 0.62 under P_{CO_2}=0.25 to 1.00 at P_{CO_2}=1 (500 mA cm^{-2}). Consequently, through modifying local CO_2 concentration, interfacial *CO/*H ratio can be deduced as fundamental drivers for alcohol formation. Either increase in *CO coverage or reduction in *H coverage can be a promising strategy to achieve a high selectivity to alcohol.

2.3. Mechanism understanding of *CO/*H coverage

To explain the variation of interfacial *CO/*H coverage under different interfacial CO_2 concentration, the mechanism was analyzed. The reaction rate for CO_2RR can be given through Butler–Volmer equation [29]:

$$R = A\theta\exp\left(\frac{-G_a^0 - e\beta U_{SHE}}{kT}\right) \quad (1)$$

in which A corresponds to prefactor, θ is the coverage of reactants, G_a^0 is the activation energy at 0 V vs. SHE, U_{SHE} is potential vs. SHE, β is the transfer coefficient, k is Boltzmann constant, and T is the reaction temperature. Through Eq. 1, under specific potential, it can be deduced that the reaction rate is intricately linked to the coverage of reactants. During CO_2RR process, the electroreduction from CO_2 to CO can be divided into four steps (detailed in SI), and the reaction ($CO_{2(g)} + e^- \rightarrow *CO_2^-$) serves as the rate-determining step. Therefore, the reaction rate for reduction from CO_2 to CO is related to P_{CO_2}. Consequently, with the increase of P_{CO_2}, the conversion rate accelerates, leading to an augmentation in interfacial $CO_{(g)}$ coverage. According to adsorption/desorption equilibrium, an increased $CO_{(g)}$ coverage corresponds to a high *CO coverage. In the electrochemical experiments, the dependence of CO production rate on the P_{CO_2} was verified at a current density of 300 mA cm^{-2} under varied P_{CO_2} conditions. The observed dependency of CO rate on P_{CO_2} exhibits characteristic behavior of a first order reaction (Fig. 3**a**). It indicates that the conversion rate to CO is primarily correlated to interfacial CO_2 concentration, agreeing with our deduced conclusion from Butler–Volmer equation (Fig. S11a). As the HER and CO_2RR are two competing reactions, it was found that the reaction rate

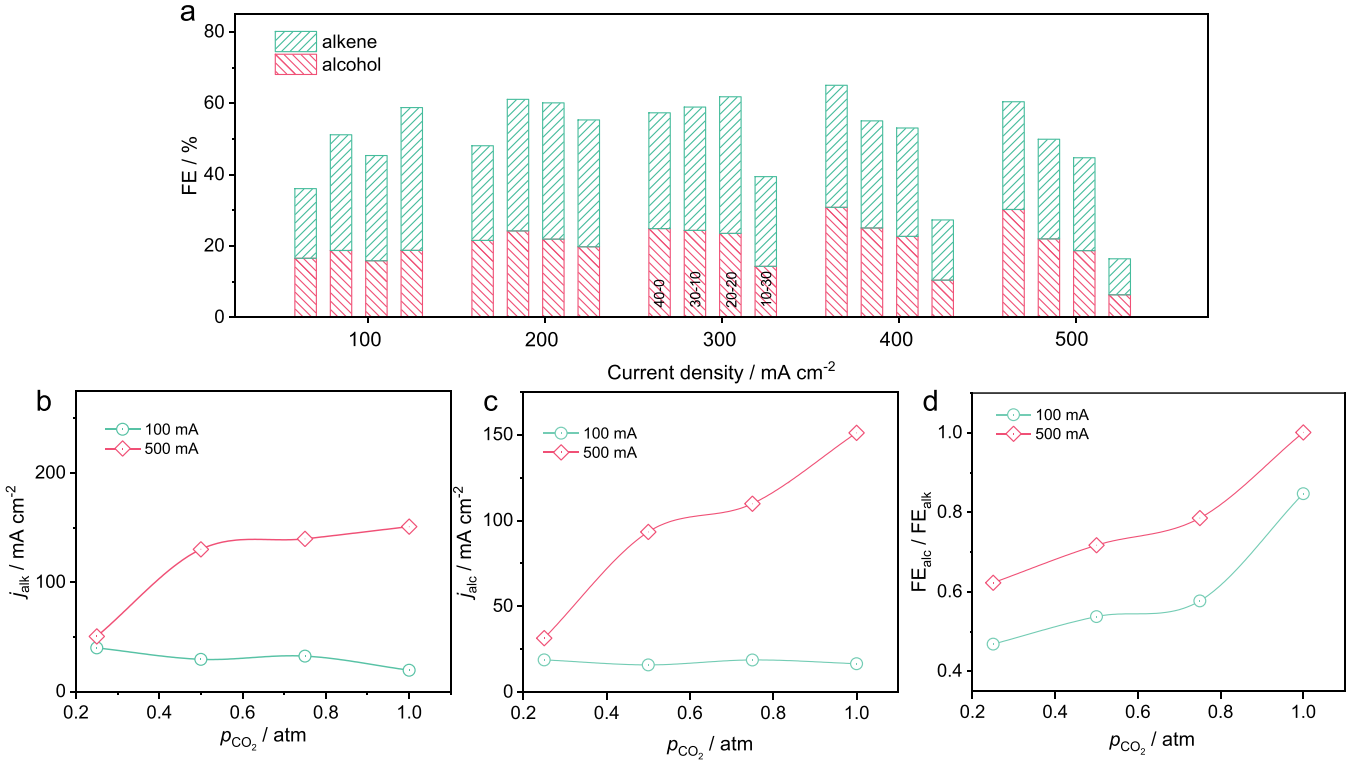

Fig. 2. Alcohol/alkene ratios dependence on *CO/*H coverage. (a) FEs of C_{2+} alcohol/alkene products at different current densities under varied P_{CO_2}. Partial current densities of (b) alkene and (c) alcohol at specific current densities. (d) Comparison of FE_{alc} to FE_{alk} with increasing P_{CO_2} at various current densities.

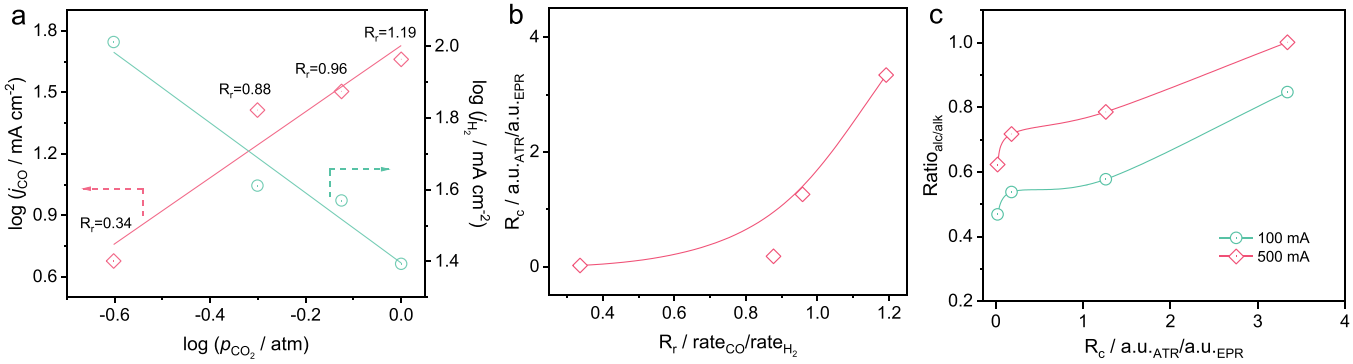

Fig. 3. Mechanism understanding of *CO/*H coverage. (a) The logarithms of j_{CO} and j_{H_2} vs. logarithms of P_{CO_2} at 300 mA cm^{-2}. Parameter R_r is employed to measure the conversion rate to CO and H_2. It is calculated as the ratio of logarithms of j_{CO} to logarithms j_{H_2}. (b) Function between R_c and R_r, and (c) relationship between R_c and Ratio$_{alc/alk}$.

to H_2 displays a typical characteristic of a negative first order reaction (Fig. S11b) [30]. That is to say that an increase of P_{CO_2} will result in a decrease in conversion rate to H_2, which is consistent with our *in-situ* EPR results. A parameter R_r, which is a ratio of conversion rate of CO to H_2 (R_r=log (j_{CO}/mA cm^{-2})/log (j_{H_2}/mA cm^{-2})), is introduced to quantify the dependence of reaction rate on P_{CO_2}. With P_{CO_2} rising from 0.25 to 1, the value for R_r increases from 0.34 to 1.19. Accordingly, an increase in R_c (*CO/*H coverage ratio) can be observed under a faster reaction rate of R_r=1.09 and finally enhance the selectivity to alcohol products (Fig. 3**b, c**). The Ratio$_{alc/alk}$ (ratio of FE$_{alc}$ to FE$_{alk}$) increases from 0.56 at R_c=0.49–0.76 under R_c=3.34 (Fig. S12), demonstrating that *CO/*H coverage ratio plays as a vital role in the formation of alcohol.

Based on *in-situ* characterizations and kinetics studies, the mechanism explaining the influence of local CO_2 concentration on products selectivity can be proposed. Since conversion rate from CO_2 to CO is a first-order reaction, interfacial CO_2 concentration determines the conversion rate from CO_2 to CO. It can be observed that effective conversion rate results in a higher interfacial *CO coverage and a lower *H coverage, contributing to a higher R_c value. The increased *CO/*H coverage ratio, in turn, facilitates the formation of alcohol.

2.4. General strategy to achieve high selectivity to alcohol

Through modulating local reaction environment, varied interfacial *CO/*H coverage can be achieved. The correlation between *CO/*H and alcohol selectivity was further established. It is revealed that R_c value, which corresponds to interfacial *CO/*H coverage ratio, is the fundamental driver for selectivity to alcohol.

A hydrophobic layer on the catalyst can effectively minimize the volume of solution in touch with electrode-electrolyte interface,

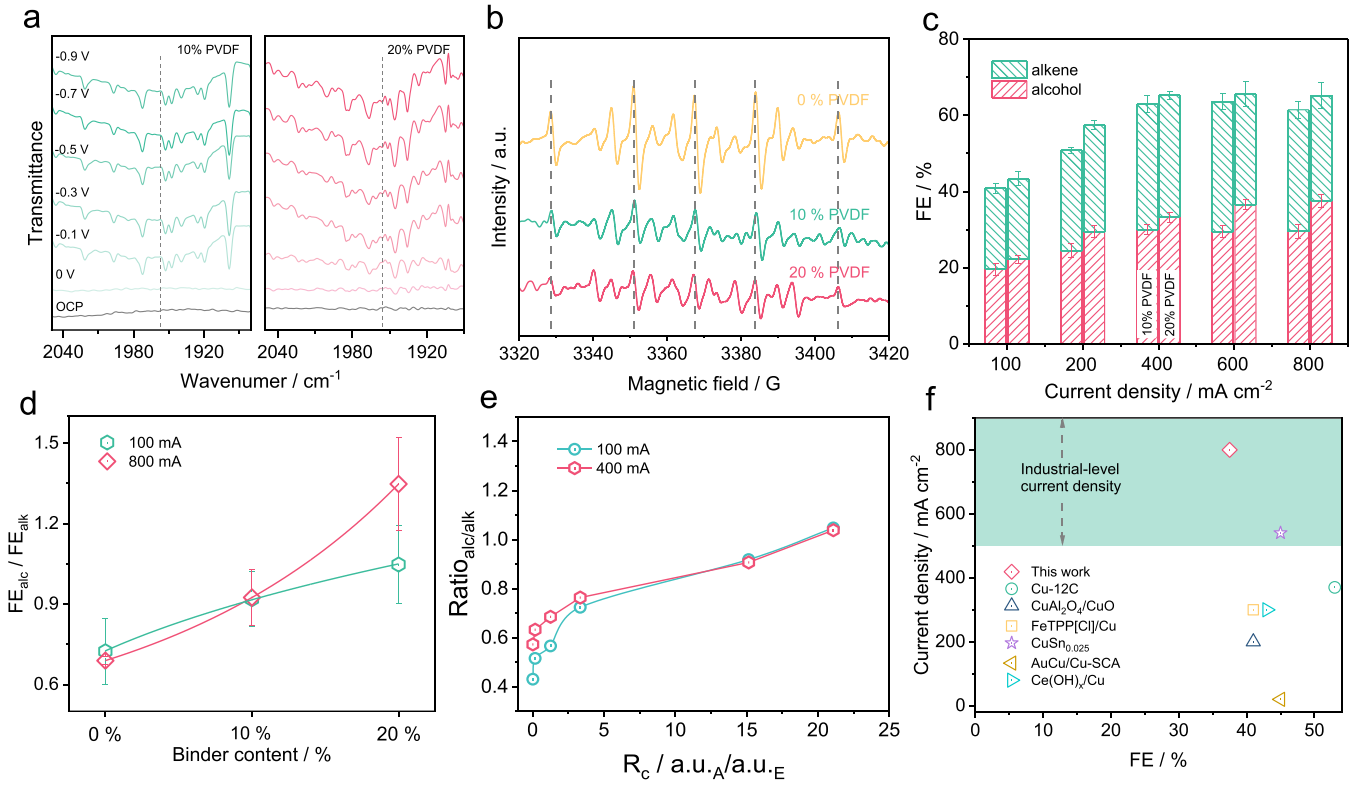

Fig. 4. General strategy to tune *CO/*H coverage. (a) The *in-situ* ATR-IR spectra and (b) *operando* EPR spectra collected on catalyst with 10 wt%/20 wt% PVDF. (c) FE$_{alc}$ and FE$_{alk}$ of Cu catalyst with varied PVDF content at different current densities. (d) The correlation between FE$_{alc}$/FE$_{alk}$ and binder content and (e) the relationship between Ratio$_{alc/alk}$ and R_c. (f) Total current density and FE$_{alc}$ of Cu with 20 wt% PVDF in comparison with other reported Cu-based catalysts.

resulting in a reduced *H coverage [31]. The decrease in competing HER activity is advantageous for the conversion from $CO_{2(g)}$ to $CO_{(g)}$, accompanied by an enhanced *CO coverage at the interface. Consequently, an increase in R_c value is realized, theoretically accelerating the selectivity to alcohol. To evaluate the deduction, a hydrophobic binder, polyvinylidene fluoride (PVDF), was added into the catalyst ink at weight ratios of 10 % or 20 %.

The commercial copper exhibits a nanoparticle structure with sizes of 50 nm (Fig. S13). A series of physicochemical characterizations confirm that the addition of PVDF into catalyst does not change the initial morphology of copper, and the element F distributes evenly on the surface (Fig. S14 and S15).

For ATR-IR spectra of catalysts containing PVDF, it can be observed that the peak corresponding to *CO becomes increasingly pronounced as more negative potentials are applied (Fig. 4**a**, Fig. S16). On the other hand, a reduction in the EPR intensity demonstrates a decreased interfacial *H coverage for catalysts with higher PVDF contents (Fig. 4**b**). These findings indicate that the introduction of PVDF binder into the catalyst can further modify local CO_2 concentration, along with an enhancement in the R_c value without influence on the electronic structure (Fig. S17).

The addition of PVDF proves effective in inhibiting the HER, leading to a decrease in j_{H_2} from 120 mA cm^{-2} to 64 mA cm^{-2} as content increasing from 0 % to 20 % (800 mA cm^{-2}) (Fig. S18). This decrease suggests a relatively lower *H coverage on the triple-phase interface. Furthermore, an increase in *CO accelerates the formation of alcohol, improving j_{alc} from 203 mA cm^{-2} to 300 mA cm^{-2} (800 mA cm^{-2}, PVDF content ranging from 0 % to 20 %) (Fig. S19a). A decrease in *H coverage is associated with a poor selectivity to alkene, leading to j_{alk} decreasing from 295 mA cm^{-2} to 222 mA cm^{-2} (Fig. S19b). These observations align with our previous findings that a high R_c value can enhance selectivity to alcohol (Fig. 4**c**). Upon plotting function between binder content and FE_{alc}/FE_{alk}, it is evident that FE_{alc}/FE_{alk} exists a positive correlation with an increase in binder content (increase from 0.69 at 0 % PVDF to 1.35 at 20 % PVDF), emphasizing the decisive role of *CO/*H coverage ratio in alcohol selectivity (Fig. 4**d,** Fig. S20). Meanwhile, through tuning P_{CO_2} coupled with modulation in interfacial hydrophobic, we succeed in elevating R_c value from 0.02 to 21.08 (Fig. S21). Furthermore, the value for $R_{alc/alk}$ experiences a notable increase, advancing from 0.43 at R_c=0.02–1.04 at R_c=21.08 (100 mA cm^{-2}, Fig. 4**e**). Importantly, in comparison with other Cu-based catalysts, device constructed with Cu containing 20 wt% PVDF delivers a high selectivity of 37.5 % to alcohol at an industrial-level current density of 800 mA cm^{-2}. A partial current density of 300 mA cm^{-2} for alcohol formation surpasses most reported catalyst-engineering materials, exhibiting a potential in industrial applications (Fig. 4**f**) [9,15, 32–34].

3. Conclusion

This work emphasizes the decisive role of *CO/*H coverage in the pathway to alcohol formation and provides a new direction for the fundamental research in the CO_2RR. Through tuning local CO_2 concentration, R_c value, a parameter to measure *CO/*H coverage, can be modulated. According to the experimental results, the selectivity between alcohol and alkene formation depends on the variance of R_c value. We validated this principle by introducing 20 wt% PVDF into the catalyst for further adjustments in interfacial CO_2 concentration. As a result, the FE for C_{2+} alcohol production maintains at 37.5 % under a high current density of 800 mA cm^{-2}, corresponding to a partial current density of 300 mA cm^{-2}. More importantly, this research points out *CO/*H coverage acting as fundamental drivers for the alcohol selectivity and proves the application potential of local environment in fundamental research.

CRediT authorship contribution statement

Chaojie Chen: Writing – original draft, Investigation, Formal analysis, Data curation. **Linsen Huang:** Investigation. **Yunling Jiang:** Investigation. **Yao Zheng:** Writing – review & editing, Supervision, Conceptualization. **Shizhang Qiao:** Writing – review & editing, Supervision, Conceptualization.

Declaration of Competing Interest

The authors declare that they have no known competing financial interests or personal relationships that could have appeared to influence the work reported in this paper.

Data availability

Data will be made available on request.

Acknowledgments

The authors gratefully acknowledge the financial support provided by the Australian Research Council through Discovery Project Programs (FT200100062, DP230102027, LP210301397, CE230100032). C.C. was supported by the Chinese CSC Scholarship Program.

Appendix A. Supporting information

Supplementary data associated with this article can be found in the online version at doi:10.1016/j.nanoen.2024.109656.

References

[1] J. Masa, C. Andronescu, W. Schuhmann, Electrocatalysis as the Nexus for sustainable renewable energy: the gordian knot of activity, stability, and selectivity, Angew. Chem. Int. Ed. Engl. *59* (36) (2020) 15298–15312, https://doi.org/10.1002/anie.202007672.

[2] G. Wang, J. Chen, Y. Ding, P. Cai, L. Yi, Y. Li, C. Tu, Y. Hou, Z. Wen, L. Dai, Electrocatalysis for CO_2 conversion: from fundamentals to value-added products, Chem. Soc. Rev. *50* (8) (2021) 4993–5061, https://doi.org/10.1039/D0CS00071J.

[3] S. Nitopi, E. Bertheussen, S.B. Scott, X. Liu, A.K. Engstfeld, S. Horch, B. Seger, I.E. L. Stephens, K. Chan, et al., Progress and perspectives of electrochemical CO_2 reduction on copper in aqueous electrolyte, Chem. Rev. *119* (12) (2019) 7610–7672, https://doi.org/10.1021/acs.chemrev.8b00705.

[4] O.S. Bushuyev, P. De Luna, C.T. Dinh, L. Tao, G. Saur, J. Van de Lagemaat, S. O. Kelley, E.H. Sargent, What should we make with CO_2 and how can we make it? Joule *2* (5) (2018) 825–832, https://doi.org/10.1016/j.joule.2017.09.003.

[5] J. Chen, L. Wang, Effects of the catalyst dynamic changes and influence of the reaction environment on the performance of electrochemical CO_2 reduction, Adv. Mater. *34* (25) (2022) e2103900, https://doi.org/10.1002/adma.202103900.

[6] I.E.L. Stephens, K. Chan, A. Bagger, S.W. Boettcher, J. Bonin, E. Boutin, A. K. Buckley, R. Buonsanti, E.R. Cave, et al., 2022 Roadmap on low temperature electrochemical CO_2 reduction, J. Phys. Energy *4* (4) (2022) 042003, https://doi.org/10.1088/2515-7655/ac7823.

[7] Y. Zheng, A. Vasileff, X. Zhou, Y. Jiao, M. Jaroniec, S.Z. Qiao, Understanding the roadmap for electrochemical reduction of CO_2 to multi-carbon oxygenates and hydrocarbons on copper-based catalysts, J. Am. Chem. Soc. *141* (19) (2019) 7646–7659, https://doi.org/10.1021/jacs.9b02124.

[8] A.J. Garza, A.T. Bell, M. Head-Gordon, Mechanism of CO_2 reduction at copper surfaces: pathways to C_2 products, ACS Catal. *8* (2) (2018) 1490–1499, https://doi.org/10.1021/acscatal.7b03477.

[9] F. Li, Y.C. Li, Z. Wang, J. Li, D.-H. Nam, Y. Lum, M. Luo, X. Wang, A. Ozden, et al., Cooperative CO_2-to-ethanol conversion via enriched intermediates at molecule–metal catalyst interfaces, Nat. Catal. *3* (1) (2019) 75–82, https://doi.org/10.1038/s41929-019-0383-7.

[10] D. Gao, I. Sinev, F. Scholten, R.M. Aran-Ais, N.J. Divins, K. Kvashnina, J. Timoshenko, B. Roldan Cuenya, Selective CO_2 electroreduction to ethylene and multicarbon alcohols via electrolyte-driven nanostructuring, Angew. Chem. Int. Ed. Engl. *58* (47) (2019) 17047–17053, https://doi.org/10.1002/ange.201910155.

[11] X. Wang, J.F. de Araujo, W. Ju, A. Bagger, H. Schmies, S. Kuhl, J. Rossmeisl, P. Strasser, Mechanistic reaction pathways of enhanced ethylene yields during electroreduction of CO_2-CO Co-feeds on Cu and Cu-tandem electrocatalysts, Nat. Nanotechnol. *14* (11) (2019) 1063–1070, https://doi.org/10.1038/s41565-019-0551-6.

[12] W. Xia, Y. Xie, S. Jia, S. Han, R. Qi, T. Chen, X. Xing, T. Yao, D. Zhou, et al., Adjacent copper single atoms promote C-C coupling in electrochemical CO_2

reduction for the efficient conversion of ethanol, J. Am. Chem. Soc. *145* (31) (2023) 17253–17264, https://doi.org/10.1021/jacs.3c04612.
[13] T. Zhang, B. Yuan, W. Wang, J. He, X. Xiang, H. Tailoring, Intermediate coverage on the $CuAl_2O_4$/CuO catalyst for enhanced electrocatalytic CO_2 reduction to ethanol, Angew. Chem. Int. Ed. Engl. *62* (29) (2023) e202302096, https://doi.org/10.1002/anie.202302096.
[14] Y. Lin, T. Wang, L. Zhang, G. Zhang, L. Li, Q. Chang, Z. Pang, H. Gao, K. Huang, P. Zhang, Z.J. Zhao, C. Pei, J. Gong, Tunable CO_2 electroreduction to ethanol and ethylene with controllable interfacial wettability, Nat. Commun. *14* (1) (2023) 3575, https://doi.org/10.1038/s41467-023-39351-2.
[15] M. Luo, Z. Wang, Y.C. Li, J. Li, F. Li, Y. Lum, D.H. Nam, B. Chen, J. Wicks, et al., Hydroxide promotes carbon dioxide electroreduction to ethanol on copper via tuning of adsorbed hydrogen, Nat. Commun. *10* (1) (2019) 5814, https://doi.org/10.1038/s41467-019-13833-8.
[16] L.R.L. Ting, O. Piqué, S.Y. Lim, M. Tanhaei, F. Calle-Vallejo, B.S. Yeo, Enhancing CO_2 electroreduction to ethanol on copper-silver composites by opening an alternative catalytic pathway, ACS Catal. *10* (7) (2020) 4059–4069, https://doi.org/10.1021/acscatal.9b05319.
[17] L. Ji, L. Li, X. Ji, Y. Zhang, S. Mou, T. Wu, Q. Liu, B. Li, X. Zhu, et al., Highly selective electrochemical reduction of CO_2 to alcohols on an FeP nanoarray, Angew. Chem. Int. Ed. Engl. *59* (2) (2020) 758–762, https://doi.org/10.1002/ange.201912836.
[18] X. Chang, J. Li, H. Xiong, H. Zhang, Y. Xu, H. Xiao, Q. Lu, B. Xu, C−C coupling is unlikely to be the rate-determining step in the formation of C_{2+} products in the copper-catalyzed electrochemical reduction of CO, Angew. Chem. Int. Ed. *61* (2) (2022) e202111167, https://doi.org/10.1002/anie.202111167.
[19] C. Chen, H. Jin, P. Wang, X. Sun, M. Jaroniec, Yao Zheng, S. Qiao, Local reaction environment in electrocatalysis, Chem. Soc. Rev. *53* (2024) 2022–2055, https://doi.org/10.1039/D3CS00669G.
[20] Z. Wang, H.F. Wang, P. Hu, Possibility of designing catalysts beyond the traditional volcano curve: a theoretical framework for multi-phase surfaces, Chem. Sci. *6* (10) (2015) 5703–5711, https://doi.org/10.1039/c5sc01732g.
[21] P. Wang, H. Yang, C. Tang, Y. Wu, Y. Zheng, T. Cheng, K. Davey, X. Huang, S. Z. Qiao, Boosting electrocatalytic CO_2-to-ethanol production *via* asymmetric C-C coupling, Nat. Commun. *13* (1) (2022) 3754, https://doi.org/10.1038/s41467-022-31427-9.
[22] C.M. Gunathunge, X. Li, J.Y. Li, R.P. Hicks, V.J. Ovalle, M.M. Waegele, Spectroscopic observation of reversible surface reconstruction of copper electrodes under CO_2 reduction, J. Phys. Chem. C *121* (22) (2017) 12337–12344, https://doi.org/10.1021/acs.jpcc.7b03910.
[23] Z. Chen, T. Wang, B. Liu, D. Cheng, C. Hu, G. Zhang, W. Zhu, H. Wang, Z.J. Zhao, J. Gong, Grain-boundary-rich copper for efficient solar-driven electrochemical CO_2 reduction to ethylene and ethanol, J. Am. Chem. Soc. *142* (15) (2020) 6878–6883, https://doi.org/10.1021/jacs.0c00971.
[24] E.L. Clark, C. Hahn, T.F. Jaramillo, A.T. Bell, Electrochemical CO_2 reduction over compressively strained CuAg surface alloys with enhanced multi-carbon oxygenate selectivity, J. Am. Chem. Soc. *139* (44) (2017) 15848–15857, https://doi.org/10.1021/jacs.7b08607.
[25] X. Feng, J. Liu, L. Chen, Y. Kong, Z. Zhang, Z. Zhang, D. Wang, W. Liu, S. Li, et al., Hydrogen radical-induced electrocatalytic N_2 reduction at a low potential, J. Am. Chem. Soc. *145* (18) (2023) 10259–10267, https://doi.org/10.1021/jacs.3c01319.
[26] Y. Wang, H. Li, W. Zhou, X. Zhang, B. Zhang, Y. Yu, Structurally disordered RuO_2 nanosheets with rich oxygen vacancies for enhanced nitrate electroreduction to ammonia, Angew. Chem. Int. Ed. Engl. *61* (19) (2022) e202202604, https://doi.org/10.1002/anie.202202604.
[27] S. Mu, H. Lu, Q. Wu, L. Li, R. Zhao, C. Long, C. Cui, Hydroxyl radicals dominate reoxidation of oxide-derived Cu in electrochemical CO_2 reduction, Nat. Commun. *13* (1) (2022) 3694, https://doi.org/10.1038/s41467-022-31498-8.
[28] M. Schreier, Y. Yoon, M.N. Jackson, Y. Surendranath, Competition between H and CO for active sites governs copper-mediated electrosynthesis of hydrocarbon fuels, Angew. Chem. Int. Ed. Engl. *57* (32) (2018) 10221–10225, https://doi.org/10.1002/anie.201806051.
[29] X. Liu, P. Schlexer, J. Xiao, Y. Ji, L. Wang, R.B. Sandberg, M. Tang, K.S. Brown, H. Peng, et al., pH effects on the electrochemical reduction of CO_2 towards C_2 products on stepped copper, Nat. Commun. *10* (1) (2019) 32, https://doi.org/10.1038/s41467-018-07970-9.
[30] X. Chang, T. Wang, Z.J. Zhao, P. Yang, J. Greeley, R. Mu, G. Zhang, Z. Gong, Z. Luo, et al., Tuning Cu/Cu_2O interfaces for the reduction of carbon dioxide to methanol in aqueous solutions, Angew. Chem. Int. Ed. Engl. *57* (47) (2018) 15415–15419, https://doi.org/10.1002/anie.201805256.
[31] D. Wakerley, S. Lamaison, F. Ozanam, N. Menguy, D. Mercier, P. Marcus, M. Fontecave, V. Mougel, Bio-inspired hydrophobicity promotes CO_2 reduction on a Cu surface, Nat. Mater. *18* (11) (2019) 1222–1227, https://doi.org/10.1038/s41563-019-0445-x.
[32] M. Li, N. Song, W. Luo, J. Chen, W. Jiang, J. Yang, Engineering surface oxophilicity of copper for electrochemical CO_2 reduction to ethanol, Adv. Sci. *10* (2) (2023) e2204579, https://doi.org/10.1002/advs.202204579.
[33] S. Shen, X. Peng, L. Song, Y. Qiu, C. Li, L. Zhuo, J. He, J. Ren, X. Liu, J. Luo, AuCu alloy nanoparticle embedded Cu submicrocone arrays for selective conversion of CO_2 to ethanol, Small *15* (37) (2019) e1902229, https://doi.org/10.1002/smll.201902229.
[34] C. Chen, X. Yan, S. Liu, Y. Wu, Q. Wan, X. Sun, Q. Zhu, H. Liu, J. Ma, L. Zheng, et al., Highly efficient electroreduction of CO_2 to C_{2+} alcohols on heterogeneous dual active sites, Angew. Chem. Int. Ed. Engl. *59* (38) (2020) 16459–16464, https://doi.org/10.1002/ange.202006847.